Enhancing 5-hydroxymethylfurfural oxidation to 2,5-furan-dicarboxylic acid with Au-supported catalysts: Optimizing reaction parameters and unraveling degradation mechanism through DFT calculations

Toyese Oyegoke, Achraf Sadier, Sara Navarro-Jaén, Alessia Ventimiglia, Nikolaos Dimitratos, Franck Dumeignil, Baba El-Yakubu Jibril, Robert Wojcieszak, Carine Michel

Catalysis Today 445 (2025) 115086

Contents lists available at ScienceDirect

Catalysis Today

journal homepage: www.elsevier.com/locate/cattod

Enhancing 5-hydroxymethylfurfural oxidation to 2,5-furan-dicarboxylic acid with Au-supported catalysts: Optimizing reaction parameters and unraveling degradation mechanism through DFT calculations

Toyese Oyegoke [a,e], Achraf Sadier [b], Sara Navarro-Jaén [b], Alessia Ventimiglia [c], Nikolaos Dimitratos [c,d], Franck Dumeignil [b], Baba El-Yakubu Jibril [e], Robert Wojcieszak [b,f,*], Carine Michel [a,**]

[a] CNRS, ENS de Lyon, LCH, UMR 5182, Lyon 69342, France
[b] Univ. Lille, CNRS, Centrale Lille, Univ. Artois, UMR 8181 - UCCS - Unité de catalyse et chimie du solide, Lille F-59000, France
[c] Dipartimento di Chimica Industriale "Toso Montanari", Alma Mater Studiorum Università di Bologna, Viale Risorgimento 4, Bologna 40126, Italy
[d] Center for Chemical Catalysis-C3, Alma Mater Studiorum Università di Bologna, Viale Risorgimento 4, Bologna 40136, Italy
[e] Chemical Engineering Department, Faculty of Engineering, Ahmadu Bello University, Samaru, Zaria 810006, Nigeria
[f] Université de Lorraine, CNRS, L2CM UMR 7053, Nancy F-54000, France

ARTICLE INFO

Keywords:
Degradation
Oxidation
Heterogeneous catalysis
Density Functional Theory
Gold nanoparticles
HMF

ABSTRACT

Lignocellulosic biomass holds promise for producing valuable chemicals. Among possible key reactions, the 5-hydroxymethylfurfural (HMF) oxidation to 2,5-furandicarboxylic acid (FDCA) using O_2 as a final oxidant and supported Au catalysts is a promising route but that suffers from carbon balance issues. This study explores the mechanism of HMF oxidation to FDCA on a Au(111) model catalyst using computational modeling. Our results identify the main intermediate (HMFCA) and the major degradation pathways from HMF and HMFCA. Since we predict a higher degradation rate for HMF, we designed an experimental two-step approach, using a low temperature to convert fully HMF and improve the carbon balance and then raising the temperature to convert the HMFCA intermediate into FDCA. This approach was successful, reaching a high yield in FDCA (>90 %) in 8 hours while keeping the carbon balance above 97 %.

1. Introduction

The utilization of bio-derived materials for chemical production is being highlighted as a sustainable substitute for petroleum-based resources. Numerous pathways involving the transformation of carbohydrates into fuels and chemicals are being explored, specifically focusing on the production of furfural and 5-hydroxymethylfurfural (HMF)[1,2]. These compounds are recognized as pivotal platform chemicals, playing a significant role in advancing bio-based fuels and chemicals [3]. Among possible transformations of HMF, its oxidation into FDCA (2,5-furan-dicarboxylic acid) is a notable reaction since FDCA is considered a highly valuable chemical [4,5]. It can serve as a precursor for synthesizing various high-performance polymers, such as polyethylene furanoate (PEF), which has garnered significant attention as a bio-based alternative to traditional plastics like PET [6].

The aerobic oxidation of HMF to FDCA typically involves the use of catalysts. Gold-based catalysts are of particular interest due to their selectivity and efficiency in this transformation [7]. They exhibit superior stability and selectivity in the aerobic oxidation of organic compounds in aqueous environments compared to liquid-phase oxidation catalysts relying on Pt and Pd [8]. This enhanced performance is attributed to their heightened resistance to leaching in water and oxidation by molecular oxygen. Still, to improve performance, they usually require the use of an alkaline environment [9]. It has been documented that the presence of a base enhances reaction rates, allows for higher feed concentrations (up to 3 %), improves product solubility in the reaction medium, and reduces FDCA adsorption on the catalyst surface [10]. Many researchers have investigated the use of environmentally friendly solvents and base-free conditions to minimize waste and simplify downstream separation processes [11]. However, low rates

* Corresponding author at: Univ. Lille, CNRS, Centrale Lille, Univ. Artois, UMR 8181 - UCCS - Unité de catalyse et chimie du solide, Lille F-59000, France.
** Corresponding author.
E-mail addresses: robert.wojcieszak@cnrs.fr (R. Wojcieszak), carine.michel@ens-lyon.fr (C. Michel).

https://doi.org/10.1016/j.cattod.2024.115086
Received 23 May 2024; Received in revised form 2 September 2024; Accepted 26 September 2024
Available online 30 September 2024

were obtained in these cases.

The HMF oxidation to FDCA proceeds through several intermediates and hence is a very interesting example of metal and conditions dependent selectivity. The reaction network is depicted in Scheme 1. The oxidation of HMF starts either with the oxidation of the alcohol side group yielding 2,5-diformyl-furan (DFF) or the oxidation of the aldehyde side group, yielding 5-hydroxymethyl-2-furancarboxylic acid (HMFCA). Using Au as a supported metal catalyst, HMFCA is generally preferred [12] and may be identified as a product if the reaction is stopped before full conversion into FDCA. Indeed, the rate-limiting step is generally the conversion of HMFCA to 5-formyl-2-furancarboxylic acid (FFCA), the penultimate intermediate on the path to FDCA. In parallel, active oxygen species need to be generated from molecular oxygen. This is a key role of the Au-supported catalyst. Working on the aerobic oxidation of glycerol catalyzed by Au-supported catalysts, Zope et al. [13] demonstrated that the oxygen atoms that are incorporated in the oxidized product mainly originate from water, not O_2. Hence, they proposed that O_2 dissociation is activated on Au in the presence of water to generate surface hydroxyls that are the active oxygen species. Gu et al. [14] later proposed a DFT investigation of this process, mimicking neutral and basic conditions. They concluded that basic conditions facilitate the O_2 bond split and hence the generation of those surface hydroxyl but also that they are key in the desorption process of carboxylate. Megías-Sayago et al. [15] show the pivotal role played by the support surface, particularly its Brönsted acidity, in the rate-limiting step of the reaction. But acidity is just one piece of this intricate puzzle. The properties of the support, including its textural, redox, and electronic characteristics, are not the only parameters that determine the efficiency of this process. The reaction conditions, pH, temperature, and pressure influence not only the accessibility of active sites but also the processes of reactive adsorption, HMF stability, product desorption, and selectivity. Yet, despite the growing recognition of these support-related factors as key influencers of catalytic activity, a comprehensive study that correlates the chemical stability of HMF over gold-based catalysts has been conspicuously absent. Therefore, this study aims to shed light on the interplay between reaction conditions and the HMF oxidation reaction. To achieve this, we investigated an Au/ZrO_2 catalyst, with focus on seeking the optimal reaction conditions to reach the best catalytic performances. To this end, comprehensive DFT studies coupled with catalytic tests were performed.

2. Materials and methods

2.1. Catalyst preparation

Au/ZrO_2 catalyst was synthesized using the sol-immobilization technique. To obtain 1 g of the catalyst with 1 % wt of metal loading, the metal precursor solution was prepared: 0.0209 g of $HAuCl_4 * 3\,H_2O$ g were dissolved in 385 mL of distilled water (1.3×10^{-4} mol L^{-1}; 5.31×10^{-5} mol) and the solution was stirred at room temperature. After that, 1.188 mL of polyvinyl alcohol (PVA) aqueous solution previously prepared (0.1010 g in 10 mL of distilled water) was added, keeping the solution stirred (PVA: Au = 1.2:1 wt ratio). After three minutes, a fresh aqueous solution of the reducing agent $NaBH_4$ was added ($NaBH_4$: Au = 5:1 molar ratio). The change of color of the solution from yellow to dark red indicates the correct formation of gold colloidal nanoparticles. After 30 min, the support ZrO_2 was added (0.99 g), and the solution was acidified with sulfuric acid under the isoelectric point of the support (pH = 5) to maximize the interaction between the nanoparticles and the support. The solution was left under stirring overnight, then it was filtered and the catalyst was washed with distilled water (about 1 L) to remove the impurities until the washing water had reached neutral pH. The catalyst was left to dry overnight at room temperature and subsequently dried in an oven for 4 h at 80 °C. The procedure is reported in Fig. 1.

2.2. Characterizations

The ICP-OES (Inductively Coupled Plasma Optical Emission Spectrometry) analysis was performed using Agilent 720-ES ICP-OES equipment combined with Vulcan 42S automated digestion system.

Transmission Electron Microscopy (TEM) images were recorded by placing a drop of the particle's dispersion in isopropanol over a carbon film supported on a copper grid. FEI Tecnai microscope was used for the recording of the images. We observed the presence of gold particles in the range of 0.9–4 nm. About 70 percent of the particles are less than or equal to 2 nm. This agreement leads to the conclusion that the gold particles have a dispersion close to 60 %. More than 600 particles were used for the distribution size studies. It was performed using Image J software.

X-ray Photoelectron Spectroscopy (XPS) analysis was performed on an XPS Kratos, Axis UltraDLD "2009" with monochromatic Al Kα (1486.6 eV) radiation as the excitation source and equipped with high-performance hemispheric analyzer. Calibration of the binding energies

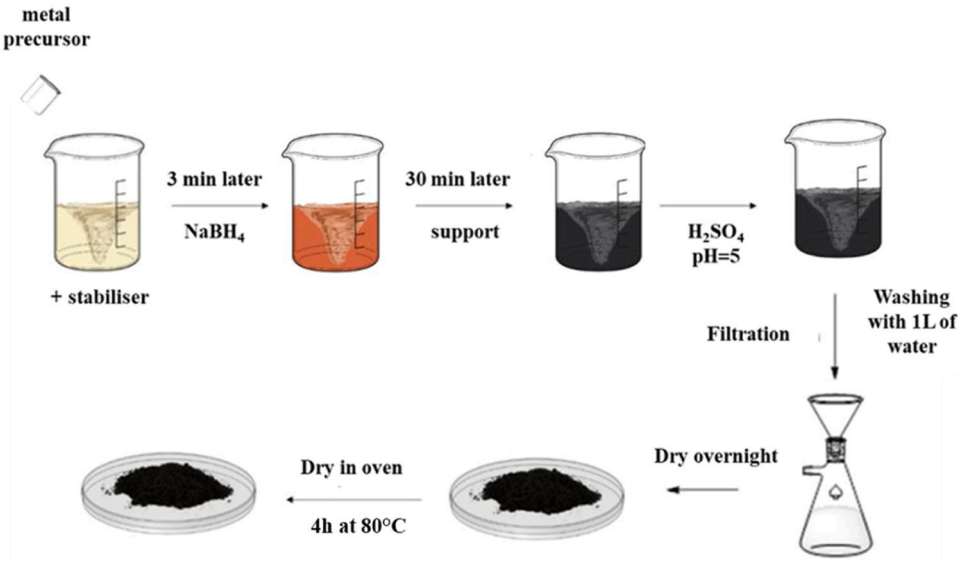

Fig. 1. Sol-immobilization methodology for Au/ZrO_2 synthesis.

was performed using the carbon C 1 s reference at 284.8 eV.

2.3. Catalytic tests

The oxidation of HMF was carried out in a 30 mL Top Industry autoclave. 20 mL of HMF aqueous solution (concentrations 45 mmol L^{-1}) and 33 mg of Au/ZrO_2 catalyst were loaded into the reactor. All tests were performed with the addition of NaOH ($n_{OH-}/n_{HMF} = 3$). After sealing, the autoclave was purged 3 times with air, pressurized with air to the required pressure ($P_{air} = 15$ bar), and finally heated to the reaction temperature (T = 50–110 °C) under stirring (600 rpm). During the experiment, liquid samples were collected to follow the kinetics of the reaction. At the end of the reaction, air was released, the reactor was cooled, and the catalyst was collected by centrifugation. The reaction products such as HMFCA, FFCA, and FDCA were analyzed by High-Performance Liquid Chromatography (HPLC, Waters 2410 RJ) equipped with RI and UV (λ = 253 nm) detectors and a Rezex ROA–organic Acid H^+ column (Ø 7.8 mm × 300 mm) at 25 °C. Diluted H_2SO_4 (5 mmol L^{-1}, 0.5 mL.min^{-1}) was used as the mobile phase. The products were identified by their retention times compared to available standards that were also used to determine the response factors.

The conversion of HMF at time t was calculated was calculated from Eq. (1):

$$Conversion_t(\%) = \frac{C_0^{HMF} - C_t^{HMF}}{C_0^{HMF}} \times 100 \quad (1)$$

where C_0^{HMF} is the initial concentration of HMF and C_t^{HMF} is the concentration of HMF at time t. The yield of product (i) is calculated using Eq. (2):

$$Yield_t^i(\%) = \frac{C_t^i}{C_0^{HMF}} \times 100 \quad (2)$$

in which C_t^i is the concentration of product (i) at a given time t.

2.4. Computational details

Periodic DFT calculations were performed using the Perdew–Burke–Ernzerhof (PBE) functional [16] with a density-dependent dispersion correction (dDsC) [17] as implemented in the Vienna Ab initio Simulation Package (VASP) package [18,19]. A tight convergence of the plane-wave expansion was obtained with a cut-off of 400 eV. The electron-ion interactions were described by the projector augmented wave method (PAW). The self-consistence field convergence criteria were set to 10^{-6} eV.

Au(111) were modeled using a p(4×4) cell, 4-layers, and a vacuum of 15 Å. The 2D Brillouin zone integration was performed at the gamma point. The bottom layers were kept frozen at the bulk position (Au-Au inter-atomic distances of 2.93 Å) while the two top layers in contact with the organic molecules were free to adjust during the geometry optimization (Conjugate-gradient algorithm). The convergence of the forces acting on atoms was set to equal or less than 0.02 eV/Å. A Monkhorst-Pack mesh K point was used for the 2D Brillouin zone integration. Transition state structures were optimized by combining the climbing image Nudged Elastic Band (CI-NEB) method [20] and the Dimer method [21]. Once the forces converged, a frequency calculation confirmed the existence of a single imaginary frequency with a normal mode corresponding to the expected reaction coordinate.

Gibbs reaction energies were evaluated at a temperature of 110 °C (or 383 K) at the standard pressure. The entropy of the surface species was neglected as well as the vibrational contribution. The rotational and translational entropies were evaluated in the rigid rotor approximation and the perfect gas approximation respectively.

3. Results and discussion

3.1. Catalyst characterizations

Fig. 2 and Fig. 3 show respectively TEM images and histogram of the mean Au particle size. From TEM images we can confirm a good dispersion of the Au nanoparticles on the zirconia support.

The histogram shows an average particle size of 5.2 ± 1.7 nm. Nanoparticles of smaller and bigger dimensions are also present (with an agglomeration of 15 nm) but in smaller quantities. In Fig. 4, TEM mapping of Au/ZrO_2 is reported, where the Au nanoparticles are highlighted in pink. The presence of ZrO_2 (O in green in Fig. 4) is also highlighted.

XPS analysis was carried out on Au/ZrO_2 to investigate the Binding Energy (BE) values of Au. In Fig. 5 the signal for Au (4 f) peaks are reported. In particular, the signal at higher energy is the 4 $f_{5/2}$, while the signal at lower energy is the 4 $f_{7/2}$. The area ratio of the two signals is ¾. From the signal 4 $f_{7/2}$ is possible to determine the oxidation state of the superficial gold: the peak is at a binding energy of 83.9 eV, indicating the presence of Au in the metallic state. It is possible to exclude the presence of Au^+ and Au^{3+} atoms because of the absence of peaks at 84.7 eV and 86 eV respectively.

3.2. Catalytic test at 110°C using Au/ZrO_2 catalyst

In Fig. 6 reports the temporal evolution of product concentrations during the oxidation of 5-hydroxymethylfurfural (HMF) on Au/ZrO_2 catalyst under the specific reaction conditions. The reaction was initiated with a relatively high initial concentration of HMF (45 mmol L^{-1}) and was conducted under air pressure (20 bar) at a temperature of 110 °C, utilizing a catalyst load of 33 mg. Notably, the conversion of HMF proceeded quite rapidly, reaching complete conversion within 2 h of reaction time. The principal product that emerged from this reaction was 5-hydroxymethyl-2-furancarboxylic acid (HMFCA), which was generated in significant quantities. Its concentration reached 12 mmol L^{-1} after 2 h. Although it displayed a slight reduction, it remained at a substantial level of 9 mmol L^{-1} by the end of the reaction. In contrast, the formation of 2,5-furan-dicarboxylic acid (FDCA) and 2-formyl-5-furancarboxylic acid (FFCA) was relatively continuous throughout the reaction, but their concentrations remained notably

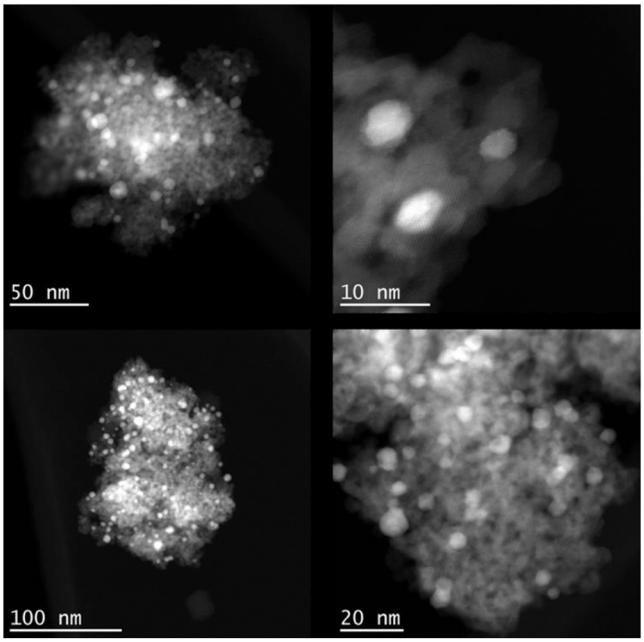

Fig. 2. TEM images for Au/ZrO_2 catalyst.

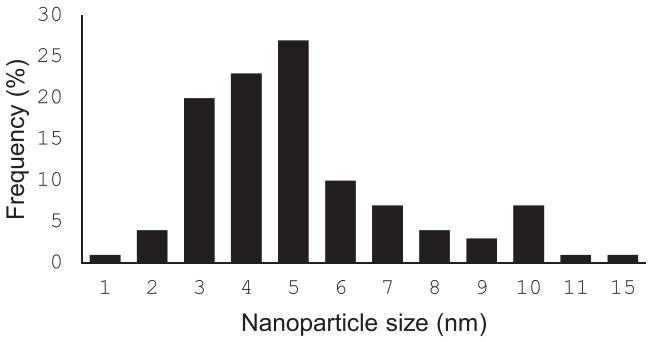

Fig. 3. Nanoparticle size distribution for Au/ZrO_2 catalyst.

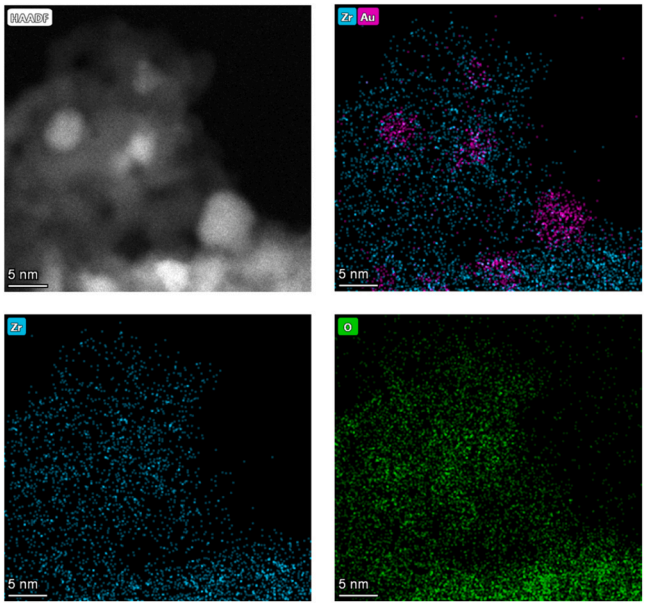

Fig. 4. TEM mapping of Au/ZrO_2 catalyst.

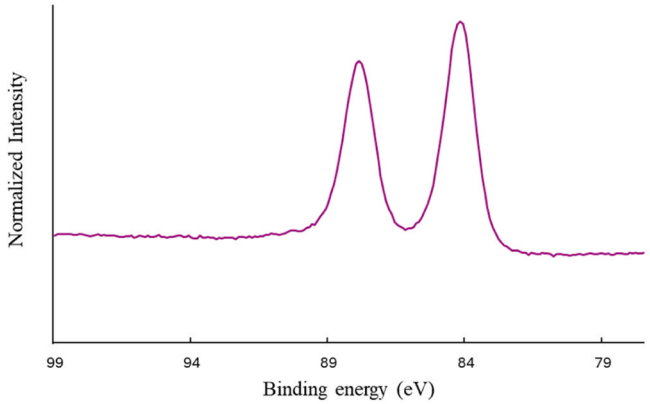

Fig. 5. : XPS Au 4 f peaks for Au/ZrO_2 catalyst.

lower compared to HMFCA, with FDCA at 3.8 mmol L^{-1} and FFCA at 1.1 mmol L^{-1}. This product distribution confirms that HMFCA was the dominant product of this catalytic process. However, a conspicuous observation was the low carbon balance of the reaction, which stood at only 32 %. This suggests that there were unaccounted carbon losses during the reaction. These discrepancies could be attributed to the thermal degradation of HMF under the reaction conditions, leading to the formation of humins and humic acid, both of which can be

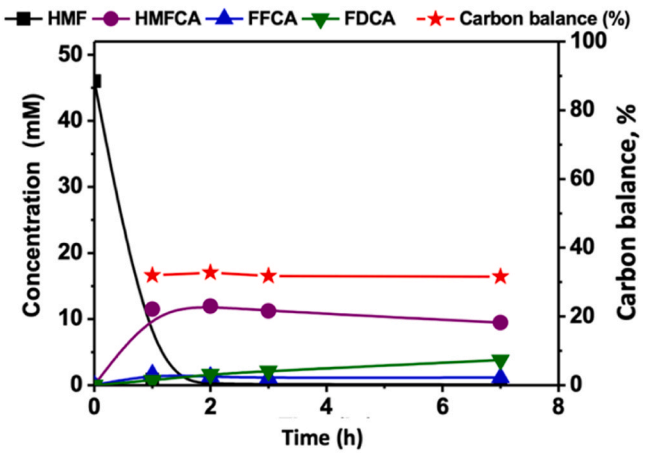

Fig. 6. : Evolutions of the concentrations of products during HMF oxidation: Concentrations are indicated as (■) HMF, (●) HMFCA, (▲) FFCA and (▼) FDCA, and (*) Carbon balance. Reaction conditions: 20 mL solution of HMF (45 mmol L^{-1}), $m_{Au/ZrO2}$ = 33 mg, PVA:Au weight ratio = 1.2, n_{HMF}/n_{Au} = 500, n_{OH-}/n_{HMF} = 3, 110 °C, 20 bar air, 7 h, 600 rpm.

considered as byproducts of the reaction. The low formation of FDCA and the prevalence of HMF degradation at 110 °C contributed to this reduced carbon balance, signifying that the fundamental reaction conditions may need further optimization to address the carbon mass balance issue and enhance the overall efficiency of the process.

The degradation of HMF due to elevated temperatures and basic conditions is a well-documented phenomenon in chemical processes [14,22,23]. HMF is susceptible to degradation under these conditions, impacting the overall yield and selectivity of reactions. At higher temperatures, HMF may undergo reactions that result in the formation of undesired byproducts, such as humins, furans, and other complex compounds. Basic conditions can further exacerbate the degradation of HMF. Under basic conditions, HMF may undergo various reactions, including isomerization, dehydration, and fragmentation, leading to the formation of less valuable products [24,25]. It is clear that to address HMF degradation optimization of reaction conditions, minimizing undesirable side reactions and maximizing the yield of target products is necessary. Therefore, understanding the mechanistic pathways of HMF degradation under different conditions is crucial for the development of more efficient and sustainable processes.

3.3. *DFT study of the degradation routes*

A better understanding of the possible degradation routes is provided here using DFT to evaluate the stability of possible intermediates on Au (111), a model surface that may very well represent the active sites found on the large Au nanoparticles as determined experimentally here. Surface intermediates are labeled with a prefix x (e.g., xOH for a chemisorbed hydroxyl or xHMF for a chemisorbed HMF).

To start, we investigated the oxidation of HMF into FDCA on Au using DFT calculations. The activation of O_2 in the presence of two water molecules can generate four surface hydroxyl ($O_2 + 2\,H_2O + 4X \rightarrow 4$ xOH, G_{rxn} = –0.97 eV) according to previous works [13,14]. In the following, we will consider xOH being the active oxygen species that can abstract a H from xHMF regenerating a water molecule or that can bind to a C of the organic moiety yielding a gem-diol or a carboxylic acid. 6 xOH are required in total to oxidize HMF into FDCA. The reaction scheme and the corresponding Gibbs reaction energies are reported in Fig. 7. The adsorption of HMF is slightly endergonic (+0.26 eV) and is followed by the oxidation of either the alcohol termination or the aldehyde termination, yielding xDFF and xHMFCA respectively. The oxidation of the aldehyde group of HMF is more exothermic than the oxidation of the alcohol group on the Au(111) surface. This is in

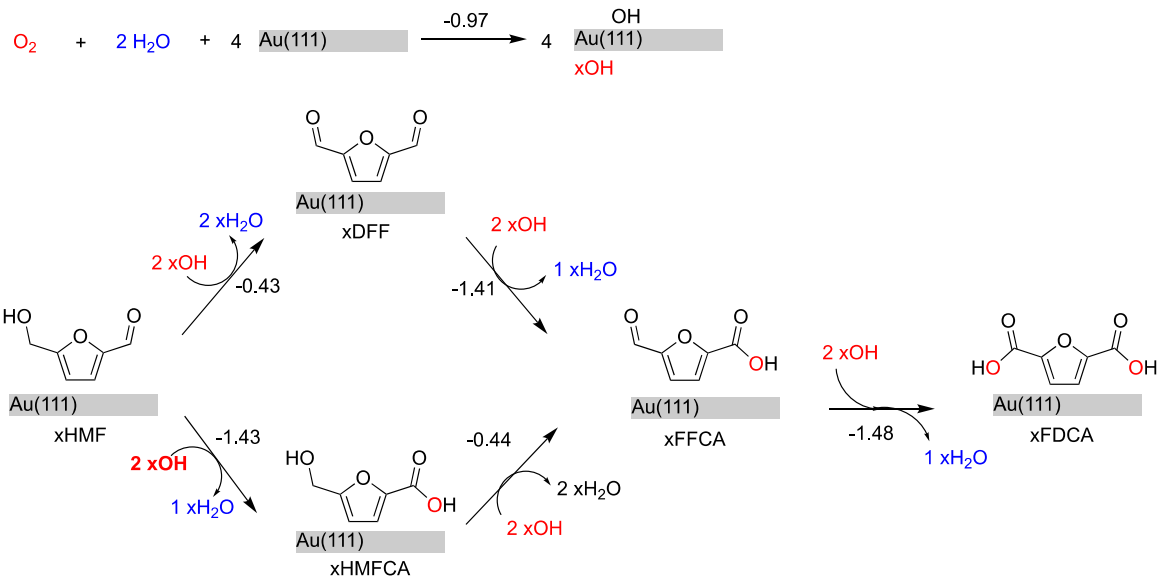

Fig. 7. Oxidation of HMF into FDCA on Au(111) using xOH as an active oxygen species. Gibbs reaction energies are indicated for each step in eV at 1 bar and 110°C. Reactions are balanced with the appropriate number of xOH, xH_2O, and pristine Au(111) slab.

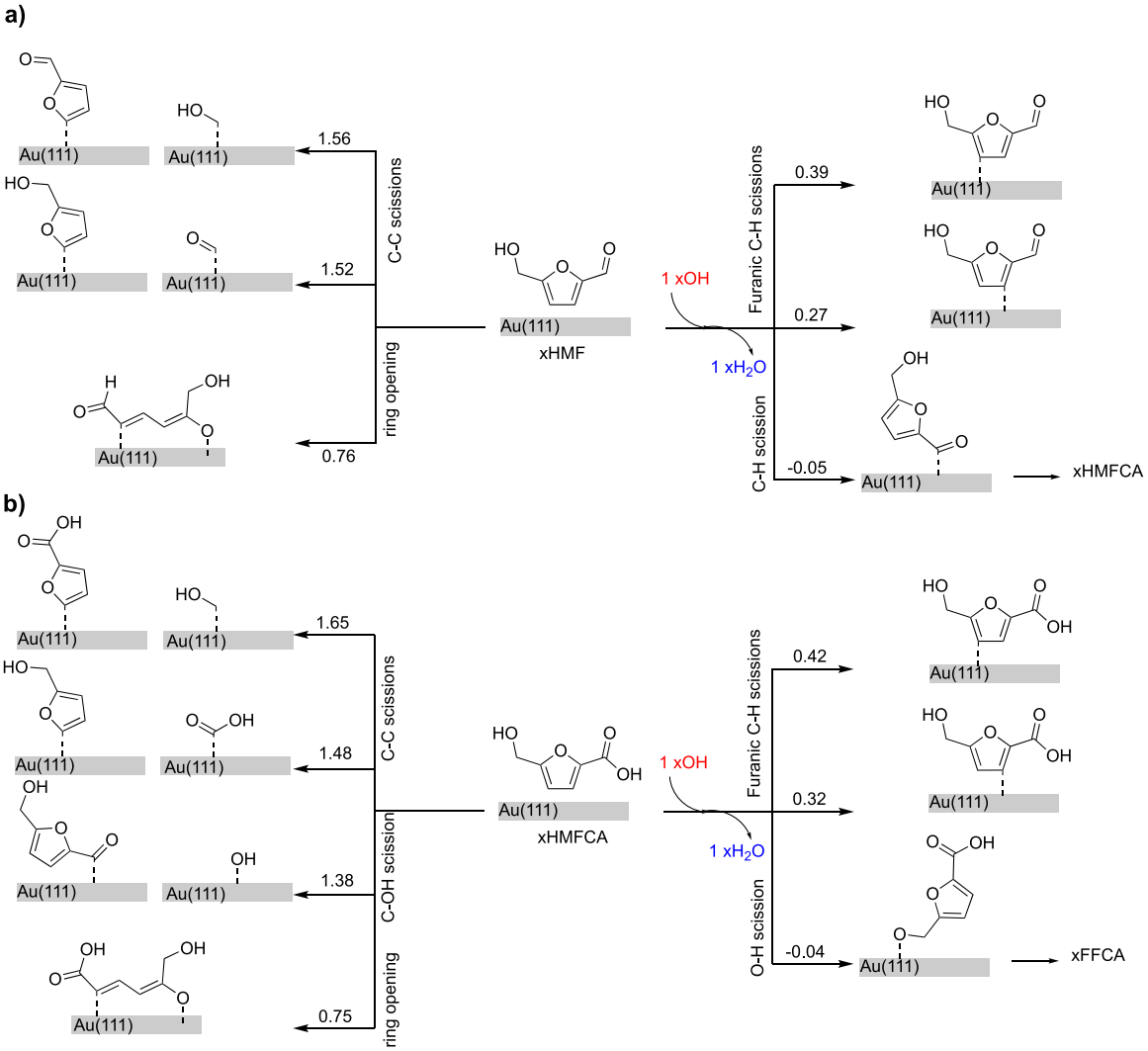

Fig. 8. Possible degradation pathways of (a) HMF and (b) HMFCA in the presence of the active species xOH on Au(111). Gibb's reaction energies are reported in eV at 110 °C and 1 bar. Reactions are balanced with the appropriate number of xOH, xH_2O, and pristine Au(111) slab.

agreement with the greater exothermicity found to oxidize acetaldehyde vs. ethanol on Au(111) (−2.02 vs. −1.21 eV) by Gu et al. [14]. Besides, the same study determines that the oxidation of acetaldehyde by xOH on Au(111) is a barrier-less process while the oxidation of ethanol is limited by the C-H bond scission (with a +0.42 eV barrier). Thus we infer that the HMF oxidation on Au(111) is predicted to process through the oxidation of the aldehyde, through the xHMFCA intermediate, which is in agreement with the experimental findings (i.e. identification of HMFCA in the course of the reaction). The next oxidation step produces FFCA, consuming again 2 xOH, a step that is exergonic (-0.44 eV from HMFCA). Finally, the remaining aldehyde group is easily oxidized (-1.48 eV) and xFDCA is obtained. The catalytic cycle closes with the exergonic desorption of FDCA and 6 water molecules, with no thermodynamic limitation along the process. The optimized structures of xHMF, xHMFCA, xDFF, xFFCA, and xFDCA are represented in SI. They are all weakly bound to the Au(111) surface, the furanic cycle parallel to the surface at around a 3 Å distance of the surface.

Possible degradation routes were explored such as (1) the two possible C-C scissions that yield the loss of one of the two substituents of the furanic ring, (2) the furanic ring opening through C-O scission and (3) the scission of the C-H bonds of the furanic ring or the aldehyde. Those degradation processes may occur starting from HMF, competing with the HMF oxidation into HMFCA but they may also happen starting from the long-lasting intermediate HMFCA, competing with its desorption and more importantly with its conversion into FFCA and then FDCA. In HMFCA, we also considered the O-H scission and the C-OH scission of the carboxylic moiety. The reaction energies of those degradation pathways are reported in Fig. 8**.** The C-C scissions are systematically strongly endothermic with reaction energies above 1.48 eV. The C-OH scission in HMFCA is also strongly endothermic (1.38 eV). As a consequence, the corresponding activation barriers are so high (above the corresponding reaction energy) that those processes are too slow to compete with the oxidation of HMF that is operated at 110 °C. In contrast, the C-H scission within the furanic ring appears as a more plausible step towards degradation, with a milder endothermicity (from +0.27 eV to +0.42 eV). Interestingly, the scission of the furanic C-H is easier in HMF (+0.27 eV, in beta position relative to the carbonyl group) than in HMFCA (+0.32 eV, in beta position relative to the carboxylic acid group). This trend is confirmed when computing the activation barriers corresponding to the H abstraction of this furanic H by xOH: the first degradation step is easier in HMF than in HMFCA, with an activation barrier of 0.71 eV vs. 0.79 eV. The structural geometries of the co-adsorbed state, the transition state, and the final state of the degradation routes for HMF and HMFCA are presented in Fig. 9. The structures are quite similar when comparing the HMF degradation route and the HMFCA degradation route. Noticeably, the transition state is earlier in HMFCA than in HMF with a shorter C–H bond (1.34 Å in HMFCA vs. 1.42 Å in HMF) and longer (HO)–H bond (1.28 Å in HMFCA vs. 1.19 Å in HMF). Finally, since the C-H scission in the furanic cycle of xHMF is below 0.75 eV, this degradation reaction is faster than the ring opening of xHMF and xHMFCA that has to overcome a barrier greater than the endothermicity of the reaction (+0.75 eV and +0.76 eV in xHMFCA and xHMF respectively).

In short, we predict that HMF is more sensitive to degradation than HMFCA and that this degradation starts with the abstraction of the furanic H in the beta position relative to the carbonyl group.

3.4. Catalytic tests in two steps

Taking into account input from DFT studies, new catalytic tests were performed aiming at limiting the degradation during the conversion of HMF into FDCA.

Firstly, the catalytic test in two isolated steps reactions was carried out (Fig. 10). The first step was performed under the same reaction conditions as previously (Fig. 6) but using a lower reaction temperature (T = 50 °C) to limit the degradation of HMF. HMF was smoothly converted to reach 100 % conversion after 7 h. HMFCA was the main product formed (41 mmol L^{-1} after 7 h) while FFCA and FDCA were minor products. As hypothesized based on our DFT calculations, the carbon balance was enhanced by 61 % (from 32 % using our initial conditions to 93 % after 7 h at 50 °C). At the end of this first step (after 7 h), the solution was recovered, a fresh catalyst was added to the reactant solution (n_{HMFCA}/n_{Au} = 500) and the temperature was increased to 110 °C. The HMFCA was totally converted at the end of this second step in 3 h. FDCA was the main product formed, with a maximum concentration reaching 40 mmol L^{-1} after 10 h. Finally, the carbon balance slightly decreased to 81 % but still remained above the one we obtained using our initial one-step strategy (32 %, see Fig. 6). This is a clear advantage of using isolated two-step reactions, converting HMF at a low temperature to avoid the formation of by-products through

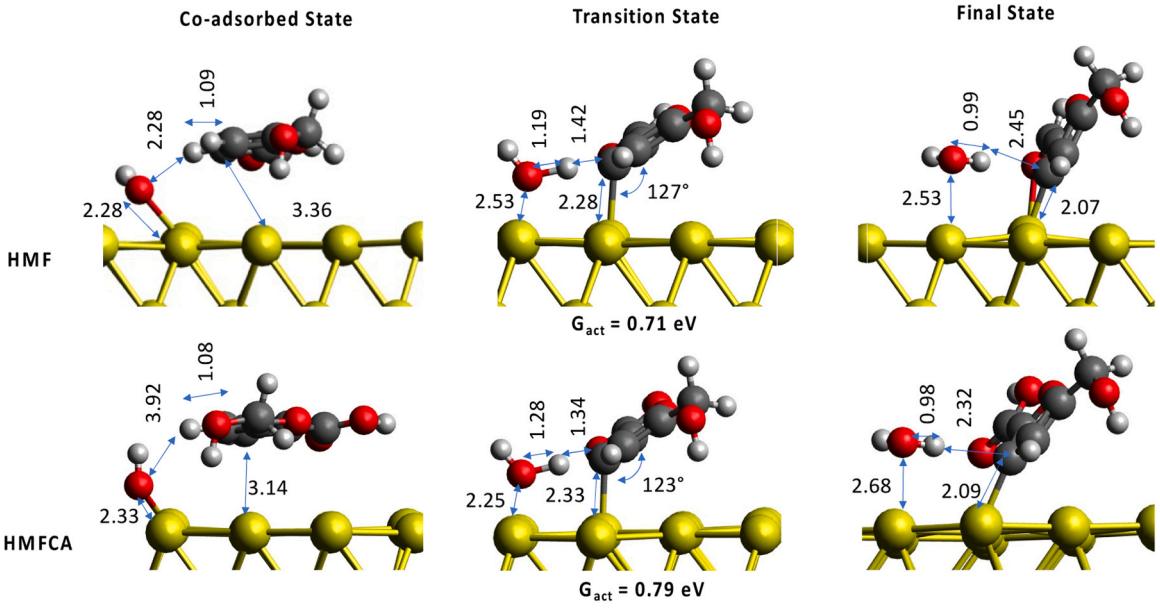

Fig. 9. Optimized structures along the furanic H abstraction by xOH in HMF and HMFCA. The H is positioned in the beta of the carbonyl in HMF and of the acid in HMFCA. Main distances are indicated in Å. Gibb's activation energy is defined using the separated reactants as a reference and is reported in eV.

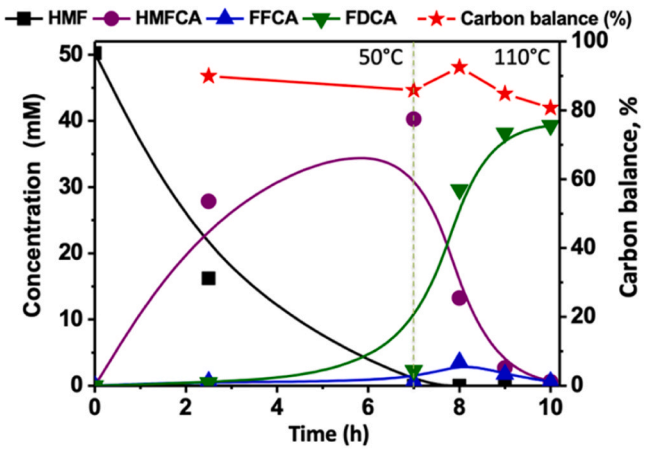

Fig. 10. Evolution of the concentrations of different products as a function of time in two isolated steps reactions with solution recovery. (■) HMF concentration, (●) HMFCA concentration, (▲) FFCA concentration, (▼) FDCA concentration (*) Carbon balance. Reaction conditions: 20 mL solution of HMF (45 mmol L^{-1}), $m_{Au/ZrO2}$ = 33 mg, PVA:Au weight ratio = 1.2, n_{HMF}/n_{Au} = 500, n_{OH-}/n_{HMF} = 3, 0–7 h at 50 °C, 7–10 h at 110 °C, 20 bar air, 7 h, 600 rpm.

degradation, recovering the solution and adding fresh catalyst, and then raising the temperature to convert HMFCA and reach a high yield in FDCA.

The two-step reaction sequence was repeated omitting the intermediate solution recovery step and using the same reaction conditions. The results are depicted in Fig. 11. As expected, the results observed after the initial step (at a temperature of 50 °C) were identical to those obtained previously. HMF underwent complete conversion within 6 hours, resulting in an HMFCA concentration of 45 mmol L^{-1}, and a remarkable 97 % carbon balance was achieved. Following this first step, the solution was not subjected to recovery, instead, a gradual temperature ramp was applied to elevate it to 110 °C. This second phase of the reaction exhibited an evolution similar to the previously isolated two-step reactions. Notably, the advantages of conducting the entire process as a one-pot reaction became evident, particularly in terms of achieving a significantly improved carbon balance, with a noteworthy 97 % balance compared to the 81 % obtained when the steps were isolated. This highlights the efficiency and advantages of a one-pot approach over the two separate-step reactions.

To further assess the sensitivity of HMF to degradation, the one-pot reaction was repeated, with no intermediate solution recovery but a rise in temperature before reaching the full conversion of HMF (Fig. 12). After 1.6 hours, a notable 68 % conversion of HMF was achieved at 50 °C, and the sole product formed was HMFCA, with a yield of 60 % (equivalent to 30 mmol L^{-1}). The carbon balance was meticulously recorded and demonstrated a commendable 97 % efficiency. At this stage, the reaction solution consisted of 32 % HMF and 63 % HMFCA. As the temperature was subsequently increased to 110 °C, the fate of HMF became apparent. It either underwent conversion into HMFCA, reaching a maximum concentration of 33 mmol L^{-1} or transformed degraded products, which contributed to a decrease in the overall carbon balance (82 % after 4.5 hours). This observation underscores the importance of fully converting all available HMF into HMFCA during the initial step of the reaction at 50 °C. Subsequently, an increase in temperature can be employed to facilitate the formation of FDCA at 110 °C, ensuring a more efficient and controlled reaction pathway.

The recyclability of the Au/ZrO_2 catalyst was studied at a reaction temperature of 50°C under 20 bar of air, utilizing NaOH as a base (as illustrated in Fig. 13). In the initial run, the catalyst exhibited robust performance, achieving a substantial 77 % conversion of HMF and yielding a 72 % HMFCA after a 2-hour reaction. For the subsequent runs, the catalyst underwent a straightforward recovery process. It was recovered through centrifugation and then subjected to an overnight drying step at 110 °C, with no additional regeneration steps. However, a noticeable decline in catalytic activity was observed during these subsequent runs. In the third run, the conversion rate dropped to 22 %. Nonetheless, it is noteworthy that throughout these recycling runs, the carbon balance was consistently maintained at levels exceeding 97 %, underscoring the efficient and sustainable nature of the catalytic process. The primary product, HMFCA, remained dominant, reinforcing the feasibility of recycling the Au/ZrO_2 catalyst for multiple reaction cycles. One recycling test on a two-step process was also performed but the overall activity followed the same deactivation trend as for the test at 50 °C. It suggests that the deactivation of the catalyst is linked probably to the deposition of carbon species on the gold surface.

4. Conclusions

The oxidation of HMF into FDCA using Au/ZrO_2 catalysts was performed at 110°C but was limited by a critically low carbon balance

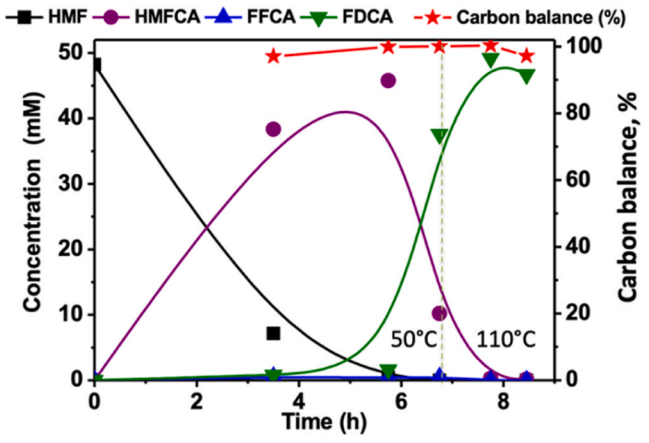

Fig. 11. Evolution of the concentrations of different products as a function of time in a one-pot reaction without solution recovery. (■) HMF concentration, (●) HMFCA concentration, (▲) FFCA concentration, (▼) FDCA concentration (*) Carbon balance. Reaction conditions: 20 mL solution of HMF (45 mmol L^{-1}), $m_{Au/ZrO2}$ = 33 mg, PVA:Au weight ratio = 1.2, n_{HMF}/n_{Au} = 500, n_{OH-}/n_{HMF} = 3, 0–6 h at 50 °C, 6–9 h at 110 °C, 20 bar air, 7 h, 600 rpm.

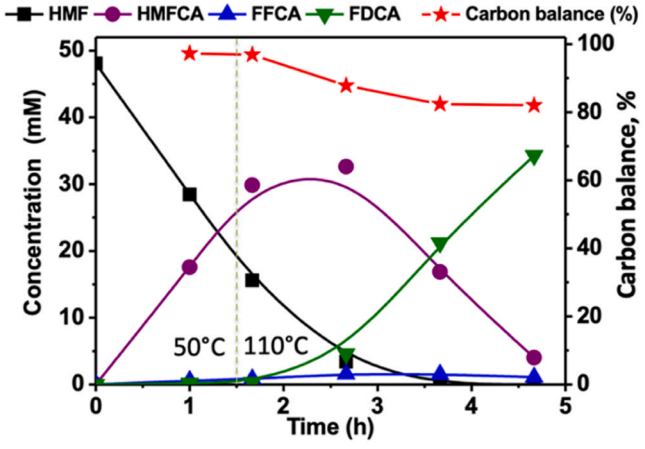

Fig. 12. : Evolution of the concentrations of different products as a function of time in a one-pot reaction without catalyst recovery. (■) HMF concentration, (●) HMFCA concentration, (▲) FFCA concentration, (▼) FDCA concentration (*) Carbon balance. Reaction conditions: 20 mL solution of HMF (45 mmol L^{-1}), $m_{Au/ZrO2}$ = 33 mg, PVA:Au weight ratio = 1.2, n_{HMF}/n_{Au} = 500, n_{OH-}/n_{HMF} = 3, 0–1.6 h at 50 °C, 1.6–4.5 h at 110 °C, 20 bar air, 7 h, 600 rpm.

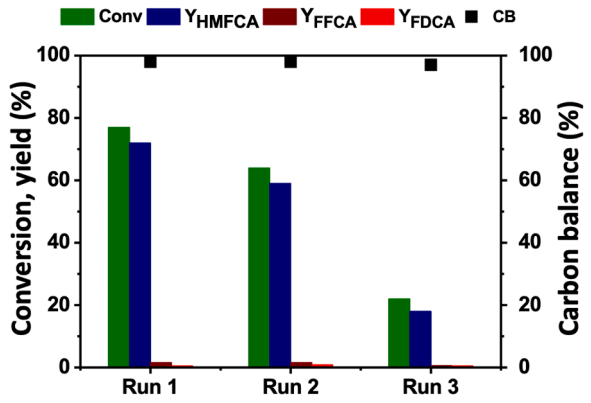

Fig. 13. : Catalyst recyclability test. Reaction conditions: 20 mL solution of HMF (45 mmol L^{-1}), $m_{Au/ZrO2}$ = 33 mg, PVA:Au weight ratio = 1.2, n_{HMF}/n_{Au} = 500, n_{OH-}/n_{HMF} = 3, 50 °C, 20 bar air, 2 h reaction, 600 rpm.

(32 %) and a low yield in the targeted product. To better understand the origin of this carbon low, the mechanism of the oxidation of HMF into FDCA on gold was investigated using periodic DFT calculations. This computational study has proven that HMF oxidation starts with the aldehyde oxidation generating HMFCA as a key intermediate that was then oxidized into FFCA and FDCA. Then, degradation routes were explored, starting from HMF and HMFCA. Based on the reaction energies, ring opening and cracking around aldehyde, hydroxyl, and acid functional groups were discarded while the hydrogen abstraction from the furan rings was identified as a major degradation route. A comparison of the degradation intensity across HMF and HMFCA on Au (111) using reaction and activation energies confirms that HMF is more prone to degradation than HMFCA on Au(111) through abstraction of the furanic H in beta to the aldehyde functional group. Those results guided the design of a two-step approach to experimentally convert HMF into FDCA while limiting carbon loss. Starting with a lower temperature (50 °C) allows to convert HMF into HMFCA with limited carbon loss. Once a full conversion in HMF is reached, raising the temperature to 110 °C allows to rapidly reach a high yield in FDCA while still maintaining the carbon balance above 97 %. Complementary tests confirmed the advantage of using a one-pot procedure vs. a two-isolated steps procedure and the importance of raising the temperature once HMF has reached a 100 % conversion. Recyclability tests confirm the robustness of this approach, keeping the carbon loss above 97 % after three runs.

CRediT authorship contribution statement

Nikolaos Dimitratos: Methodology, Investigation, Data curation, Conceptualization. **Dumeignil Franck:** Resources, Project administration, Funding acquisition, Conceptualization. **Baba El-Yakubu Jibril:** Writing – review & editing, Validation, Supervision. **Toyese Oyegoke:** Writing – original draft, Visualization, Investigation. **Achraf Sadier:** Investigation, Data curation. **Sara Navarro Jaen:** Visualization, Validation, Supervision, Methodology, Investigation, Formal analysis, Data curation, Conceptualization. **Alessia Ventimiglia:** Methodology, Investigation, Data curation, Conceptualization. **Robert Wojcieszak:** Writing – review & editing, Writing – original draft, Validation, Supervision, Resources, Project administration, Methodology, Funding acquisition, Formal analysis, Data curation, Conceptualization. **carine michel:** Writing – review & editing, Validation, Supervision, Resources, Project administration, Methodology, Funding acquisition, Data curation, Conceptualization.

Declaration of Competing Interest

The authors declare the following financial interests/personal relationships which may be considered as potential competing interests. Carine MICHEL reports financial support was provided by French National Research Agency. Toyese Oyegoke reports financial support was provided by Petroleum Technology Development Fund. If there are other authors, they declare that they have no known competing financial interests or personal relationships that could have appeared to influence the work reported in this paper

Data availability

Optimized structures are provided as supplementary materials.

Acknowledgments

The financial support for this work was provided by the French National Research Agency (ANR) through the IngenCat project (ANR-20-CE43–0014) and Petroleum Technology Development Fund Nigeria (PTDF/ED/OSS/PHD/TO/1538/19). We gratefully acknowledge support from the PSMN (Pôle Scientifique de Modélisation Numérique) of the ENS de Lyon for the computing resources.

Supplementary Materials

Optimized structures are provided as supplementary materials.

Appendix A. Supporting information

Supplementary data associated with this article can be found in the online version at doi:10.1016/j.cattod.2024.115086.

References

[1] I. Itabaiana Junior, M. Avelar Do Nascimento, R.O.M.A. De Souza, A. Dufour, R. Wojcieszak, Levoglucosan: a promising platform molecule? Green Chem. 22 (2020) 5859–5880, https://doi.org/10.1039/D0GC01490G.
[2] R.J. Van Putten, J.C. Van Der Waal, E. De Jong, C.B. Rasrendra, H.J. Heeres, J. G. De Vries, Hydroxymethylfurfural, a versatile platform chemical made from renewable resources, Chem. Rev. 113 (2013) 1499–1597, https://doi.org/10.1021/CR300182K.
[3] D.A. Giannakoudakis, V. Nair, A. Khan, E.A. Deliyanni, J.C. Colmenares, K. S. Triantafyllidis, Additive-free photo-assisted selective partial oxidation at ambient conditions of 5-hydroxymethylfurfural by manganese (IV) oxide nanorods, Appl. Catal. B 256 (2019) 117803, https://doi.org/10.1016/J.APCATB.2019.117803.
[4] C. P. Ferraz, N.J.S. Costa, E. Teixeira-Neto, Â.A. Teixeira-Neto, C.W. Liria, J. Thuriot-Roukos, M.T. Machini, R. Froidevaux, F. Dumeignil, L.M. Rossi, R. Wojcieszak, 5-hydroxymethylfurfural and furfural base-free oxidation over AuPd embedded bimetallic nanoparticles, Catalysts 10 (2020) 75, https://doi.org/10.3390/CATAL10010075.
[5] R. Wojcieszak, I. Itabaiana, Engineering the future: perspectives in the 2,5-furandicarboxylic acid synthesis, Catal. Today 354 (2020) 211–217, https://doi.org/10.1016/J.CATTOD.2019.05.071.
[6] F. Drault, Y. Snoussi, S. Paul, I. Itabaiana, R. Wojcieszak, Recent advances in carboxylation of furoic acid into 2,5-furandicarboxylic acid: pathways towards bio-based polymers, ChemSusChem 13 (2020) 5164–5172, https://doi.org/10.1002/CSSC.202001393.
[7] C.P. Ferraz, M. Zieliński, M. Pietrowski, S. Heyte, F. Dumeignil, L.M. Rossi, R. Wojcieszak, Influence of support basic sites in green oxidation of biobased substrates using Au-promoted catalysts, ACS Sustain Chem. Eng. 6 (2018) 16332–16340, https://doi.org/10.1021/ACSSUSCHEMENG.8B03330/ASSET/IMAGES/MEDIUM/SC-2018-03330P_0008.GIF.
[8] H.K. Al Rawas, C.P. Ferraz, J. Thuriot-Roukos, S. Heyte, R. Wojcieszak, S. Paul, Influence of Pd and Pt promotion in gold based bimetallic catalysts on selectivity modulation in furfural base-free oxidation, Catalysts 11 (2021) 1226, https://doi.org/10.3390/CATAL11101226.
[9] N. Capece, A. Sadier, C. Palombo Ferraz, J. Thuriot-Roukos, M. Pietrowski, M. Zieliński, S. Paul, F. Cavani, R. Wojcieszak, Aerobic oxidation of 1,6-hexanediol to adipic acid over Au-based catalysts: the role of basic supports, Catal. Sci. Technol. 10 (2020) 2644–2651, https://doi.org/10.1039/D0CY00183J.
[10] Y. Li, X. Ma, W. Lv, H. Chen, L. Yu, Z. Ma, S. Wang, Y. Li, Efficient selective oxidation of 5-hydroxymethylfurfural with oxygen over a ZnCrAl mixed oxide catalyst derived from hydrotalcite-like precursor, Ind. Eng. Chem. Res 61 (2022) 11597–11603, https://doi.org/10.1021/ACS.IECR.2C00886/ASSET/IMAGES/LARGE/IE2C00886_0006.JPEG.
[11] J. Thuriot-Roukos, C.P. Ferraz, H. K. Al Rawas, S. Heyte, S. Paul, I. Itabaiana, M. Pietrowski, M. Zieliński, M.N. Ghazzal, F. Dumeignil, R. Wojcieszak, Supported gold catalysts for base-free furfural oxidation: the state of the art and machine-

learning-enabled optimization, Materials 16 (2023) 6357, https://doi.org/10.3390/MA16196357.
[12] B. Sang, J. Li, X. Tian, F. Yuan, Y. Zhu, Selective aerobic oxidation of the 5-hydroxymethylfurfural to 2,5-furandicarboxylic acid over gold nanoparticles supported on graphitized carbon: study on reaction pathways, Mol. Catal. 470 (2019) 67–74, https://doi.org/10.1016/J.MCAT.2019.03.026.
[13] B.N. Zope, D.D. Hibbitts, M. Neurock, R.J. Davis, Reactivity of the gold/water interface during selective oxidation catalysis, Science 330 (2010) 74–78, https://doi.org/10.1126/SCIENCE.1195055/SUPPL_FILE/ZOPE.SOM.PDF.
[14] Q. Gu, P. Sautet, C. Michel, Unraveling the role of base and catalyst polarization in alcohol oxidation on Au and Pt in water, ACS Catal. 8 (2018) 11716–11721, https://doi.org/10.1021/ACSCATAL.8B03494/SUPPL_FILE/CS8B03494_SI_001.PDF.
[15] C. Megías-Sayago, A. Lolli, S. Ivanova, S. Albonetti, F. Cavani, J.A. Odriozola, Au/Al2O3 – Efficient catalyst for 5-hydroxymethylfurfural oxidation to 2,5-furandicarboxylic acid, Catal. Today 333 (2019) 169–175, https://doi.org/10.1016/J.CATTOD.2018.04.024.
[16] E. Fabiano, L.A. Constantin, F.Della Sala, Generalized gradient approximation bridging the rapidly and slowly varying density regimes: a PBE-like functional for hybrid interfaces, Phys. Rev. B Condens Matter Mater. Phys. 82 (2010) 113104, https://doi.org/10.1103/PHYSREVB.82.113104/FIGURES/5/MEDIUM.
[17] S.N. Steinmann, C. Corminboeuf, Comprehensive benchmarking of a density-dependent dispersion correction, J. Chem. Theory Comput. 7 (2011) 3567–3577, https://doi.org/10.1021/CT200602X/SUPPL_FILE/CT200602X_SI_001.PDF.
[18] G. Sun, J. Kürti, P. Rajczy, M. Kertesz, J. Hafner, G. Kresse, Performance of the Vienna ab initio simulation package (VASP) in chemical applications, J. Mol. Struct.: Theochem 624 (2003) 37–45, https://doi.org/10.1016/S0166-1280(02)00733-9.
[19] J. Hafner, Ab-initio simulations of materials using VASP: density-functional theory and beyond, J. Comput. Chem. 29 (2008) 2044–2078, https://doi.org/10.1002/JCC.21057.
[20] G. Henkelman, B.P. Uberuaga, H. Jónsson, A climbing image nudged elastic band method for finding saddle points and minimum energy paths, J. Chem. Phys. 113 (2000) 9901, https://doi.org/10.1063/1.1329672.
[21] G. Henkelman, H. Jónsson, A dimer method for finding saddle points on high dimensional potential surfaces using only first derivatives, J. Chem. Phys. 111 (1999) 7010, https://doi.org/10.1063/1.480097.
[22] N. Mittal, M. Kaur, V. Singh, Mild and selective catalytic oxidation of 5-HMF to 2,5-FDCA over metal loaded biomass derived graphene oxide using hydrogen peroxide in aqueous media, Mol. Catal. 546 (2023) 113223, https://doi.org/10.1016/J.MCAT.2023.113223.
[23] L. Yu, H. Chen, Z. Wen, X. Ma, Y. Li, Y. Li, Solvent- and base-free oxidation of 5-hydroxymethylfurfural over a PdO/AlPO4-5 catalyst under mild conditions, Ind. Eng. Chem. Res 60 (2021) 13485–13491, https://doi.org/10.1021/ACS.IECR.1C01911/SUPPL_FILE/IE1C01911_SI_001.PDF.
[24] S. Liu, Y. Zhu, Y. Liao, H. Wang, Q. Liu, L. Ma, C. Wang, Advances in understanding the humins: formation, prevention and application, Appl. Energy Combust. Sci. 10 (2022) 100062, https://doi.org/10.1016/J.JAECS.2022.100062.
[25] K. Tashiro, M. Kobayashi, K. Nakajima, T. Taketsugu, Computational survey of humin formation from 5-(hydroxymethyl)furfural under basic conditions, RSC Adv. 13 (2023) 16293–16299, https://doi.org/10.1039/D3RA02870D.